Volume 9, Issue 6, 2019, 4671 - 4684 ISSN 2069-5837
Biointerface Research in Applied Chemistry
www.BiointerfaceResearch.com
https://doi.org/10.33263/BRIAC96.671684
Original Research Article Open Access Journal
Received: 31.10.2019 / Revised: 15.11.2019 / Accepted: 16.11.2019 / Published on-line: 21.11.2019

Computational investigation on the molecular interactions between MDM2 and its photoactivatable inhibitor

Pundarikaksha Das [1], Venkata Satish Kumar Mattaparthi [1,*]
[1]Molecular Modelling and Simulation Laboratory, Department of Molecular Biology and Biotechnology, Tezpur University, Tezpur-784 028, Assam, India
*corresponding author e-mail address: ***mvenkatasatishkumar@gmail.com, venkata@tezu.ernet.in*** | Scopus ID 54962670000

ABSTRACT
The Murine Double Minute 2 (MDM2) protein is a crucial negative regulator of the tumor suppressor p53 molecule. In order to restrict p53 functioning, MDM2 molecules are overproduced in many human tumors. Thus, reactivating p53 in cancer cells using inhibitors, disrupting p53-MDM2 binding, can offer an effective approach for cancer therapy. Recently a photoactivatable MDM2 inhibitor, a photoremovable-protecting group (PPG) in complex with idasanutlin has been reported to exert no functional effect on cellular outgrowth but allows for the selective, non-invasive activation of antitumor properties due to the release of active inhibitor idasanutlin from the complex upon irradiation with 400 nm light. In this study, using molecular docking and Molecular Dynamics (MD) simulations, we have investigated the interaction of (i) PPG-idasanutlin complex and (ii) the active inhibitor idasanutlin with MDM2 at the molecular level. We noticed that the PPG-idasanutlin complex fails to fit into the binding cavity of MDM2. But the active inhibitor idasanutlin when it is free from PPG was found to fit perfectly into the binding cavity of MDM2. From the Dictionary of Secondary Structure of Proteins (DSSP) analysis, we found that the number of α-helices, which aid in the stability of protein, were found to be more in the MDM2-idasanutlin complex rather than in the MDM2-PPG-idasanutlin complex. Using the PDBsum server, we have compared the interaction profiles of MDM2-PPG-idasanutlin, MDM2-idasnautlin and MDM2-p53 complexes. From the interaction profile, we found the active inhibitor, idasanutlin free from PPG to bind to the region in MDM2 where p53 prefers to bind.. Our findings from this study would shed light on designing more potent photoactivatable MDM2 inhibitors.
Keywords: *photoremovable-protecting group; Molecular Dynamics simulation; active inhibitor idasanutlin.*

1. INTRODUCTION
At present, cancer is one of the most dominant causes of death across the world. Many different types of cancer treatment have been developed, but the type of treatment that an individual receives depends solely on two factors: (i) the type of cancer and (ii) the stage of cancer. These treatments can be either in a single formulation or in a combination, such as immunotherapy, targeted therapy, hormone therapy, and the most common method: surgery with chemotherapy and/or radiation therapy. But these methods come with certain drawbacks, wherein the inherent toxicity and the associated adverse effects account for the majority of the drawbacks in cancer chemotherapy. To overcome the problems concerning these selectivity issues, the focus has been now shifted to exploring the targeting pathways that are exclusive for cancer cells [1-3]. Therefore targeting the cancer cell-specific protein-protein interactions (PPIs) is an effective strategy for controlling these cellular pathways, , hence paving a way for a novel targeting strategy in anticancer treatment.

One of the most targeted proteins in developing anti-cancer therapy is p53, which functions as tumor suppressor protein and is well-known to exhibit a variety of PPIs. It plays an important role in many cell-regulating pathways like DNA repair, apoptosis, cell cycle control, and cellular stress responses [4,5]. p53, when activated by different kinds of stresses, can drive cellular senescence and at times leading to apoptosis. This property has deep involvement in cancer treatment because the upregulation of p53 protein expression can instigate senescence or apoptosis in the cycling cells [6-9].

The Murine Double Minute 2 (MDM2) is an E3 ubiquitin-protein ligase. MDM2 is well studied as the primary repressor of the p53 protein activity. The mechanism of repression includes the interaction of MDM2 with p53 by promoting its ubiquitination followed by subsequent degradation by the proteasome [10-12]. The other two mechanisms by which MDM2 inhibits p53 activity are either by directly binding to and blocking the N-terminal transcriptional activation domain of p53 or by promoting the export of p53 from the nucleus to the cytoplasm [13]. This regulation of the PPI between p53 and MDM2 can play a vital role in the development of anticancer drugs.

Recently, many classes of chemical compounds have been found to be effective as MDM2 antagonists, including Nutlin-Type Compounds, Imidazoles, Imidazothiazoles, Benzodiazepines, Spirooxindoles, Isoindolones, Indole-2-Carboxylic Acid Derivatives, Pyrrolidinones, Pyrrolidines, Isoquinolines and Piperidinones, Peptides and some miscellaneous compounds [14]. The antagonist that shows the maximum number of van der Waals interactions with MDM2 will effectively be able to inhibit the PPI between MDM2-p53 [15]. Among the mentioned compounds, ntlins have been found to be the most effective in modulating the tumor-suppressing pathway of p53 [16-18]. This function is achieved by the binding of MDM2 to p53, because of which the proteolytic breakdown of p53 gets inhibited. Once p53 gets stabilized, it stops the rapid cell division, leading to cell senescence [8].

Photopharmacological strategies [19,20] can be introduced for (i) increasing the selectivity of certain MDM2 inhibitors; and (ii) making them involved as research tools to understand MDM2−p53 interactions. In photopharmacological strategies, a drug can be modified with a photoswitch [19,20], or

photoremovable-protecting group (PPG) [21-23]. The functioning of a PPG includes protecting the functional group in the pharmacophore and exhibiting selective light-triggered activation. Ideally, a photo protected drug remains in an inactive state. However, when photo-activated, the active drug is liberated [24,25].

Recently, Hansen and his group [26] described the photoactivation of the photoactivatable MDM2 inhibitor PPG-idasanutlin in hindering the binding of MDM2 and p53. They reported that idasanutlin, when bound to a PPG cannot block the interaction between MDM2 and p53, leading to p53 degradation.

But the release of the active inhibitor idasanutlin from the PPG-idasanutlin complex in a light-triggered manner (upon 400 nm irradiation) prevents the interaction between MDM2 and p53, resulting in either senescence or cell death [26]. Here, we demonstrate the molecular interaction profile of MDM2 with (i) PPG-idasanutlin complex and (ii) the active inhibitor idasanutlin (free from PPG).

2. MATERIALS AND METHODS

The 3-D structure of MDM2 bound to the transactivation domain of p53 protein (PDB ID: 1YCR) was obtained from the RCSB Protein Data Bank (PDB) [27]. The structure was then visualized using the UCSF Chimera software v.1.13.1 [28] and the MDM2 protein from the MDM2-p53 complex was separated and was saved as a new file. The 3-D structure of idasanutlin (PubChem CID: 53358942), the inhibitor molecule, was procured from the PubChem server [29] in SDF file format and then PDB file format for the same was obtained using the open Babel online server [30]. The photo-protective group (PPG) was designed in the MolView online server [31] and then saved in mol format. The mol format of PPG was then converted to pdb file format using the open Babel online server. Idasanutlin and PPG were then joined using the ArgusLab visualization software v.4.0.1 [32], followed by the energy optimization of the PPG-idasanutlin complex by the UFF (universal force field). The complex was saved in mol format initially and then converted to pdb file format using the open Babel online server.

The PatchDock web server [33] was used to prepare the MDM2-idasanutlin and MDM2-PPG-idasanutlin complexes. The geometric surface docking algorithm is the working principle of the PatchDock server. The unwanted models have been filtered out based on the clustering root-mean-square deviations (RMSD) [34] value of 1.5 Å. Ten model complexes of MDM2-idasanutlin and MDM2-PPG-idasanutlin have been obtained from the PatchDock web server. Based on the highest surface area and the lowest atomic contact energy, the best docked model of the MDM2-idasanutlin and MDM2-PPG-idasanutlin complex were selected for the study.

The MD simulation study on three systems: (i) MDM2 (Apo), (ii) MDM2-idasanutlin, and (iii) MDM2-PPG-idasanutlin was then performed using the Assisted Model Building with Energy Refinement (AMBER) 14 software package [35], where ff99SB force field [36] parameters were used for the protein part of the system, while the ligands (idasanutlin and PPG-idasanutlin) were treated with the generalized AMBER force field (GAFF) [37] parameters. The proportionate partial atomic charges of the ligands were fixed with the AM1-BCC function of the ANTECHAMBER module [38] of the AMBER14 software package. Using the xLEaP module, we have built the initial required coordinate and the topology files for all the three systems. Then the charges on each of these three systems have been neutralised by adding the counter-ions, followed by the solvation using three-site transferrable intermolecular potential (TIP3P) water molecules in a cubical box with a buffer size of 10 Å from the solute in x, y, and z-axis.

Next, the solvated structures were subjected to the two-step energy minimization process (to remove bad contacts) that includes 500 steps of steepest descent (SD) method by holding the solute with restraint followed by another 500 steps of conjugate gradient (CG) method without any restraint on the solute. During the energy minimization, 8 Å was considered as the cut off for the non-bonded interactions. The heating dyanmics was carried out for all the systems to reach the temperature gradually from 0-300 K. The generated ensemble was then subjected to equilibration for 100 ps using the NPT conditions (300 K and 1 atm pressure). Then 40 ns MD production runs were carried out for all three systems.

During the course of simulations, the periodic boundary conditions (PBC) and other electrostatic interactions were maintained using the Particle Mesh Ewald (PME) method [39,40] under isothermal and isobaric conditions, respectively. The temperature was controlled using Berendsen thermostat [41,42] to restrain all the bonds.

The stability and dynamics of the three systems were studied by analyzing their corresponding MD trajectories using the PTRAJ (Process TRAJectory) and CPPTRAJ (PTRAJ in C++) modules [43] of the AMBER14 software package. We have also carried out hydrogen bond analysis for the three systems. While calculating the number of inter and intra-molecular hydrogen bonds in the three systems, we have set the cutoff for the angle and distance to be 120^{o} and 3.5 Å respectively. The 3-D structure of the three systems were examined using the UCSF Chimera package, version 1.13.1 and VMD v.1.9.3 [44].

Using the RMSD clustering algorithm, the lowest energy conformers for both the systems: (i) MDM2-idasanutlin and (ii) MDM2-PPG-idasanutlin were taken from the highly populated clusters. The lowest energy conformer were then submitted to the PDBsum server [45-47] to study the interaction profile (residues involved in the interaction, atoms in residues involved in the interaction, types of bonds, bond lengths, etc.) between MDM2 and idasanutlin, as well as between MDM2 and PPG-idasanutlin.

3. RESULTS

We have performed MD simulation on three systems: (i) MDM2 (Apo), (ii) MDM2-idasanutlin, and (iii) MDM2-PPG-idasanutlin. To verify the accuracy of our NPT simulation algorithm, we have plotted the density, temperature, pressure, potential energy, kinetic energy and total energy of the corresponding three systems as a function of the simulation time

period (as shown in Supplementary Figure S1, S2, S3, and S4 respectively). From the plots, we can see all three systems have reached the desired temperature (300 K), pressure (1 atm), and density (1 g cc^{-1}). After equilibration, the three systems were subjected to MD simulation run for 40 ns. During the 40 ns of simulation time, the three systems (MDM2 (Apo), MDM2-idasanutlin, and MDM2-PPG-idasanutlin) have undergone rapid change in the conformations as shown in Figure 1, 2, and 3 respectively. Various structural properties such as root mean square deviation (RMSD), root mean square fluctuation (RMSF), Radius of Gyration (Rg), solvent accessible surface area (SASA), number of intramolecular and intermolecular hydrogen bonds, and the secondary structural elements were evaluated separately for the three systems. The RMSD graphs were plotted for Cα atoms of all three systems as shown in Figure 4a. For all the three systems, we observed RMSD oscillate rapidly till 10 ns of simulation time and then found settled for the rest of the simulation time. The average RMSD value of MDM2 (Apo), MDM2-idasanutlin and MDM2-PPG-idasanutlin were found to be 1.44 ± 0.25 Å, 1.41 ± 0.16 Å, and 1.35 ± 0.19 Å, respectively. Among the three systems, the MDM2-idasanutlin complex was found to be more stable in comparison with MDM2 (Apo) and MDM2-PPG-idasanutlin. Then we determined the Residue flexibility in all the three systems using RMSF analysis. Figure 4b shows the RMSF values for C-α atoms of the corresponding three systems. The average RMSF values of all the C-α atoms was found to be 0.89 ± 0.42 Å, 0.83 ± 0.32 Å, and 0.80 ± 0.31 Å for MDM2 (Apo), MDM2-idasanutlin, and MDM2-PPG-idasanutlin, respectively. From the RMSF plot, we see fluctuation of C-α atoms in the MDM2 (Apo) state to be higher than in the MDM2-idasanutlin and MDM2-PPG-idasanutlin states. Rg is another important geometrical parameter, which indicates the compactness of a system over a period of simulation time. For a protein molecule to be stable, it should maintain its compactness in an optimal temperature and pressure conditions. The average Rg values for MDM2 (Apo), MDM2-idasanutlin and MDM2-PPG-idasanutlin were found to be 13.04 ± 0.10 Å, 13.03 ± 0.07 Å, and 12.95 ± 0.08 Å, respectively. We see the size of MDM2 to maintain the same value even upon binding to idasanutlin and PPG-idasanutlin (Figure 4c). The solvent accessible surface area (SASA) gives an overview of the behavior of residues with respect to solvent, and determines the stability of the protein. The SASA for MDM2 (Apo), MDM2-idasanutlin and MDM2-PPG-idasanutlin were calculated to be 5777.98 ± 2000.05 $Å^2$, 5808.40 ± 183.78 $Å^2$, and 5894.16 ± 183.20 $Å^2$, respectively. From the SASA plot, we can infer that MDM2 has undergone subtle change in conformation upon binding with idasanutlin and PPG-idasanutlin (Figure 4d). The average structural properties of MDM2 (Apo), MDM2-idasanutlin complex, and MDM2-PPG-idasanutlin complex that were obtained from the analysis of their corresponding MD trajectories have been summarized in the Table 1.

Additionally, we also carried out the analysis of intra and inter-molecular hydrogen bonds (shown in Figure 5 and 6 respectively) present in the three systems. The number of hydrogen bonds was observed to be within the ideal range as proposed for the globular proteins [48]. From the plot, we have calculated the average number of intramolecular hydrogen bonds in MDM2 (Apo), MDM2-idasanutlin and MDM2-PPG-idasanutlin and the values were found to be 35.70 ± 4.26, 35.40 ± 4.31, and 36.60 ± 4.29, respectively (Figure 5). Figure 6 represents the intermolecular hydrogen bond analysis in the case of (a) MDM2-idasanutlin complex, and (b) MDM2-PPG-idasanutlin complex. The average number of intermolecular hydrogen bonds in (a) MDM2-idasanutlin complex, and (b) MDM2-PPG-idasanutlin complex was found to be 2 and 4 respectively. Although the number of inter-molecular hydrogen bonds in MDM2-PPG-idasanutlin complex was observed to be more than in MDM2-idasanutlin complex, we noticed that idasanutlin free from PPG actually binds to the region where p53 binds. Then we carried out the analysis of the probable secondary structure that each residue of MDM2 can adopt in (i) MDM2 (Apo), (ii) MDM2-idasanutlin, and (iii) MDM2-PPG-idasanutlin systems (Figure 7). From Figure 7, we infer that the structure of MDM2 to have more helical content in the presence of active inhibitor idasanutlin. Then we performed the Dictionary of Secondary Structure of Proteins (DSSP) analysis [49] using the Kabsch and Sander algorithm [49] to investigate the changes in secondary structural elements in the MDM2 molecule (as shown in Figure 8). From Figure 8, it can be observed that MDM2 (Apo), MDM2-idasanutlin complex and MDM2-PPG-idasanutlin complex show a noticeable difference in the number of turns and α-helices. We see more turns in MDM2 (Apo), followed by the MDM2-PPG-idasanutlin complex, and MDM2-idasanutlin complex. We also found the helical content to be higher in the MDM2-idasanutlin complex, followed by the MDM2-PPG-idasanutlin complex, and MDM2 (Apo) (Figure 8).

From the PDBsum analysis of the MDM2-idasanutlin and MDM2-PPG-idasanutlin complexes, we have studied the protein-ligand interaction profiles (as shown in Supplementary Table S1 and Table S2). The MDM2-p53 interaction profile was obtained by uploading the experimentally determined 3-D structure of the MDM2-p53 complex obtained from RSCB PDB (ID: 1YCR) in the PDBsum server (as shown in Figure 9). The interactions noticed in the MDM2-idasanutlin, MDM2-PPG-idasanutlin and MDM2-p53 complexes were summarized in Table 2.

From Table 2, we see almost the same set of MDM2 residues were involved in the interaction with p53 and idasanutlin.

To have an apparent view on the binding of idasanutlin on MDM2, we have extracted the most stable conformer (using RMSD clustering method) from the corresponding 40 ns MD simulation trajectories of the two systems (i) MDM2-idasanutlin, and (ii) MDM2-PPG idasanutlin. Using UCSF Chimera v 1.13.1 [50] we have visualized the extracted stable conformer of MDM2-idasanutlin, and MDM2-PPG idasanutlin complexes, and also the MDM2-p53 complex (PDB ID: 1YCR) obtained from RCSB PDB. We have then super-imposed the 3-D structure of MDM2-idasanutlin complex with MDM2-PPG-idasanutlin to see the differences in the binding pattern (Figure 10a). In addition we also super-imposed the 3-D structure of MDM2-idasanutlin complex with the MDM2-p53 complex to compare the binding pattern (Figure 10b).

From Figure 10a, it can be observed that the aromatic rings of idasanutlin (red) fit perfectly into the binding cavity of MDM2. However, when idasanutlin is bound to the PPG (green), it undergoes probable conformational changes, for which the

aromatic rings of idasanutlin cannot fit into the binding cavity of MDM2. From **Figure 10b**, it can be clearly seen that idasanutlin (red) occupies the binding cavity of MDM2 in the same manner as p53 (blue). Thus, it can be inferred that idasanutlin can act as a potent inhibitor, and it has the ability to disrupt the p53-MDM2 interaction.

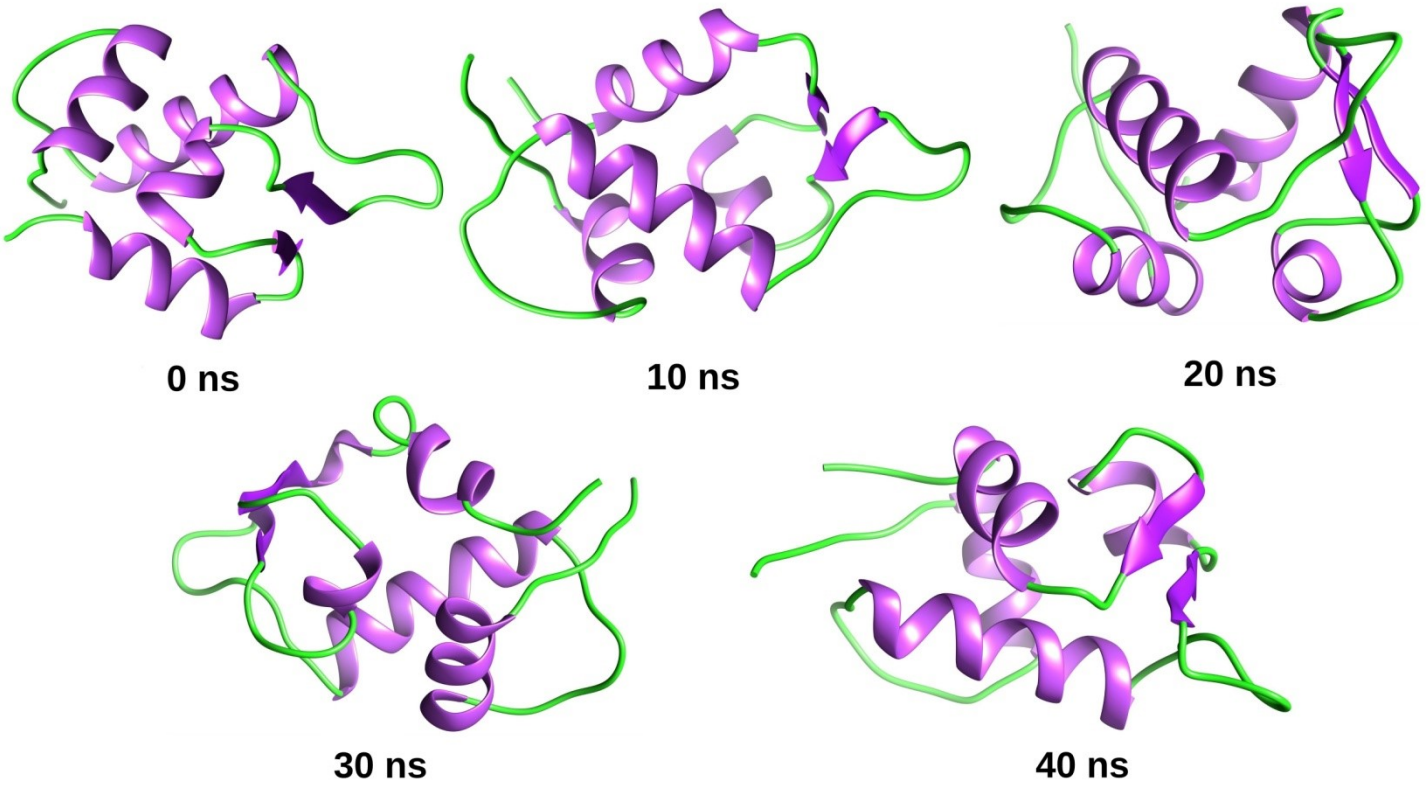

Figure 1. Conformations of MDM2 (Apo) at different time intervals of simulation.

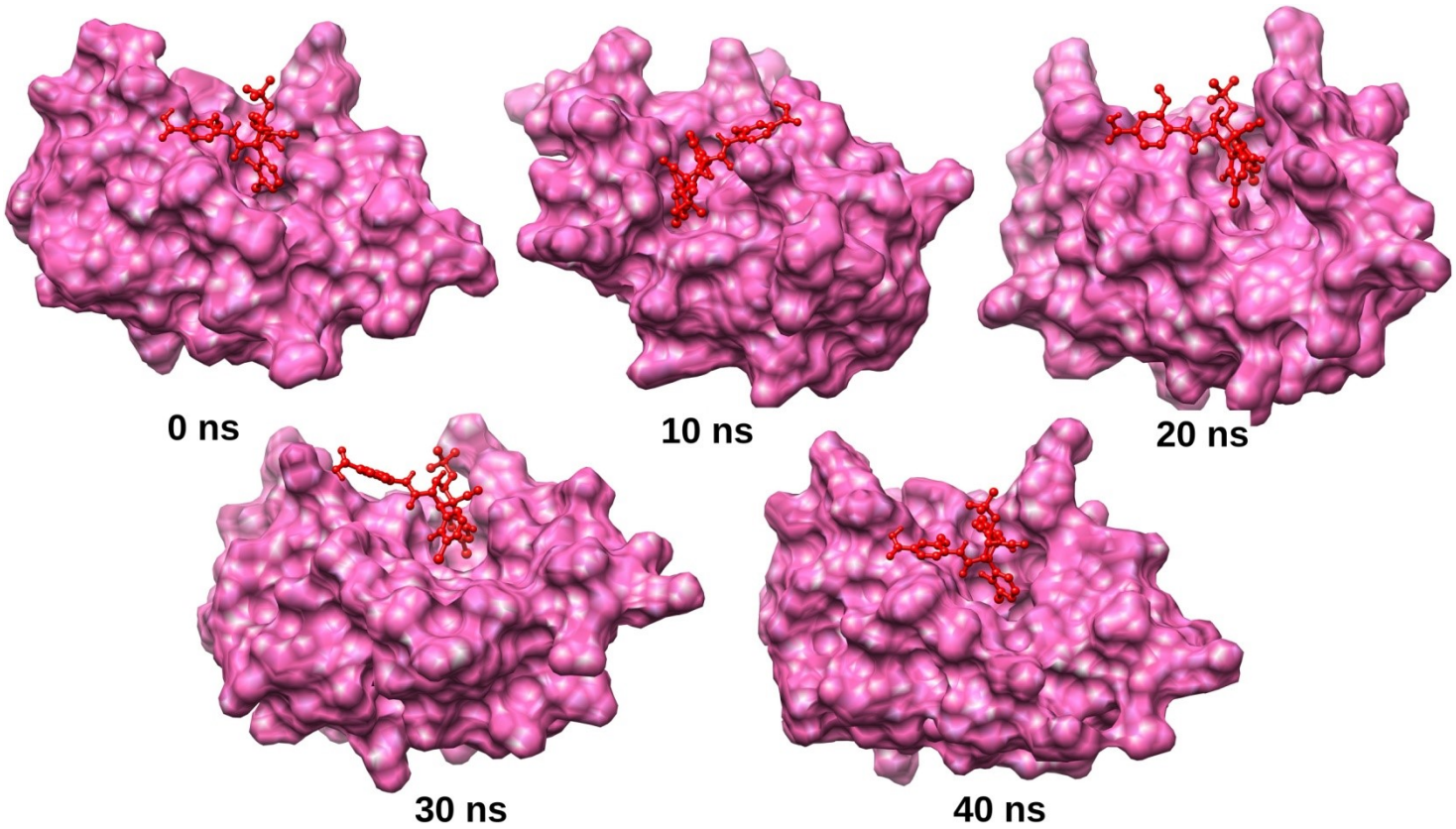

Figure 2. Conformations of MDM2-idasanutlin complex at different time intervals of simulation.

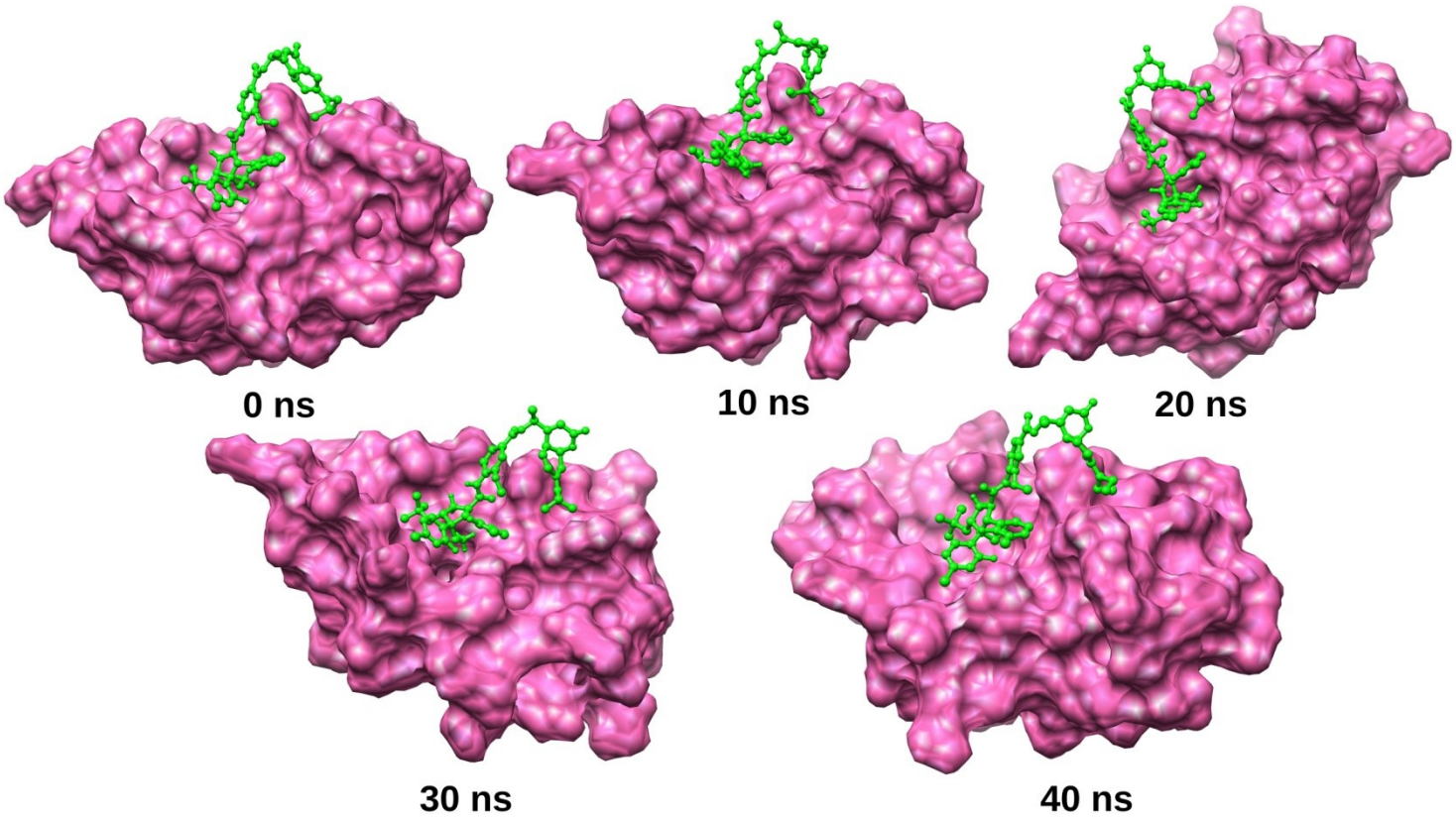

Figure 3. Conformations of MDM2-PPG-idasanutlin complex at different time intervals of simulation.

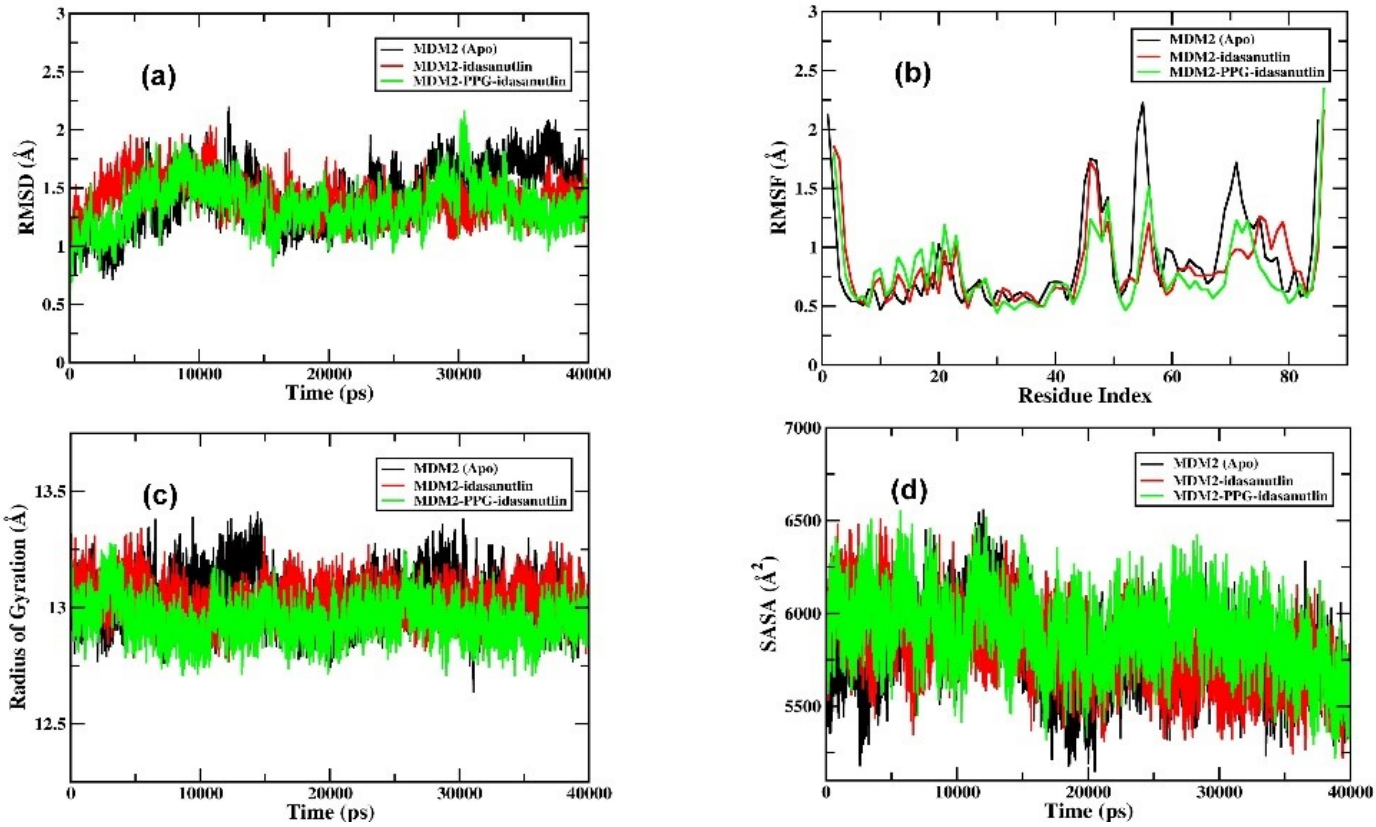

Figure 4. The structural characteristics (a) Root Mean Square Deviation (RMSD), (b) Root Mean Square Fluctuation (RMSF), (c) Radius of Gyration (Rg), and (d) Solvent Accessible Surface Area (SASA) of MDM2 (Apo), MDM2-idasanutlin, and MDM2-PPG-idasanutlin during 40 ns Molecular Dynamics simulation.

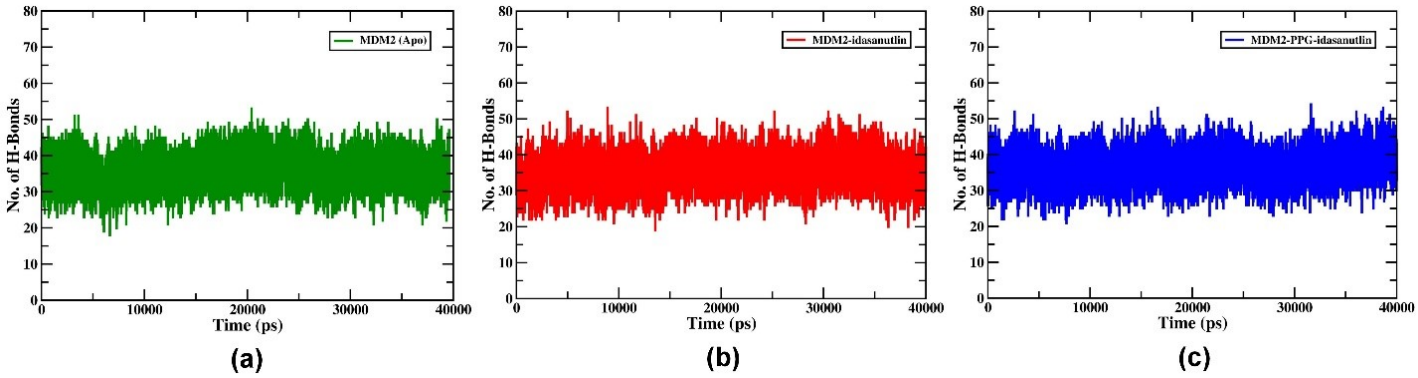

Figure 5. Intra-molecular hydrogen bond analysis for MDM2 in (a) MDM2 (Apo); (b) MDM2-idasanutlin complex; and (c) MDM2-PPG-idasanutlin complex.

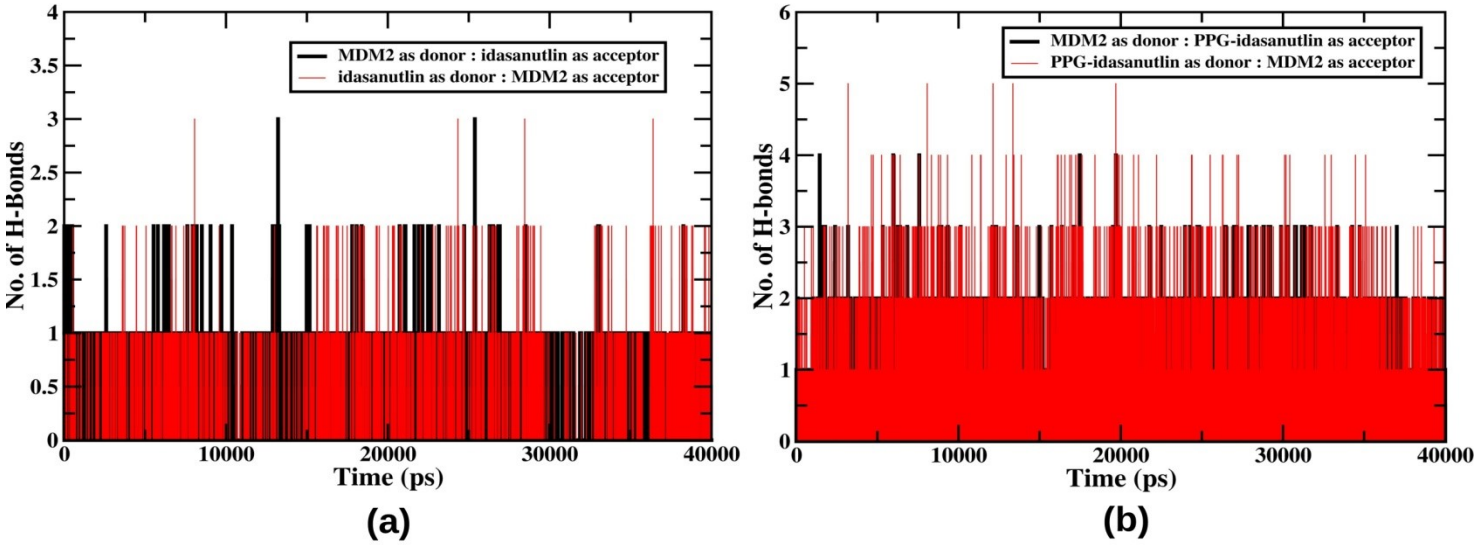

Figure 6. Inter-molecular hydrogen bond analysis for (a) MDM2-idasanutlin complex; and (b) MDM2-PPG-idasanutlin complex.

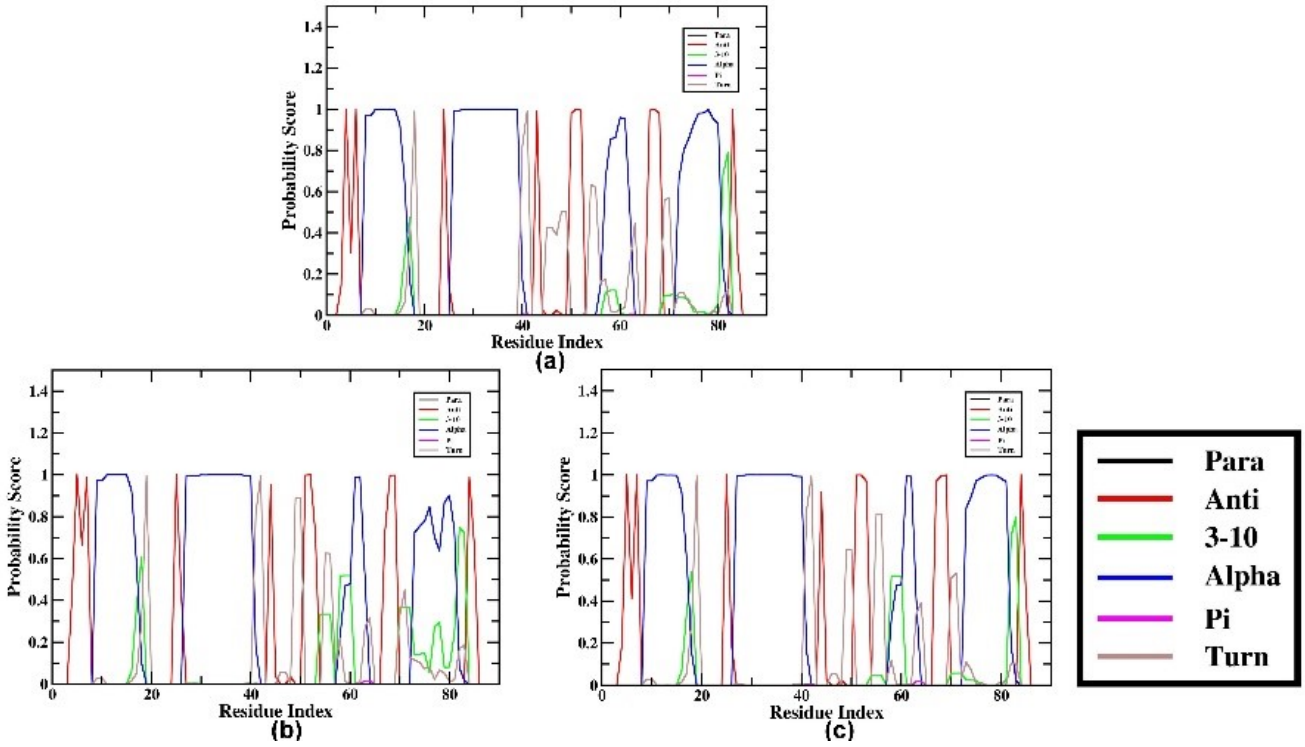

Figure 7. Probable Secondary structure score for MDM2 in (a) Apo, (b) complex with idasanutlin, and (c) complex with PPG-idasanutlin

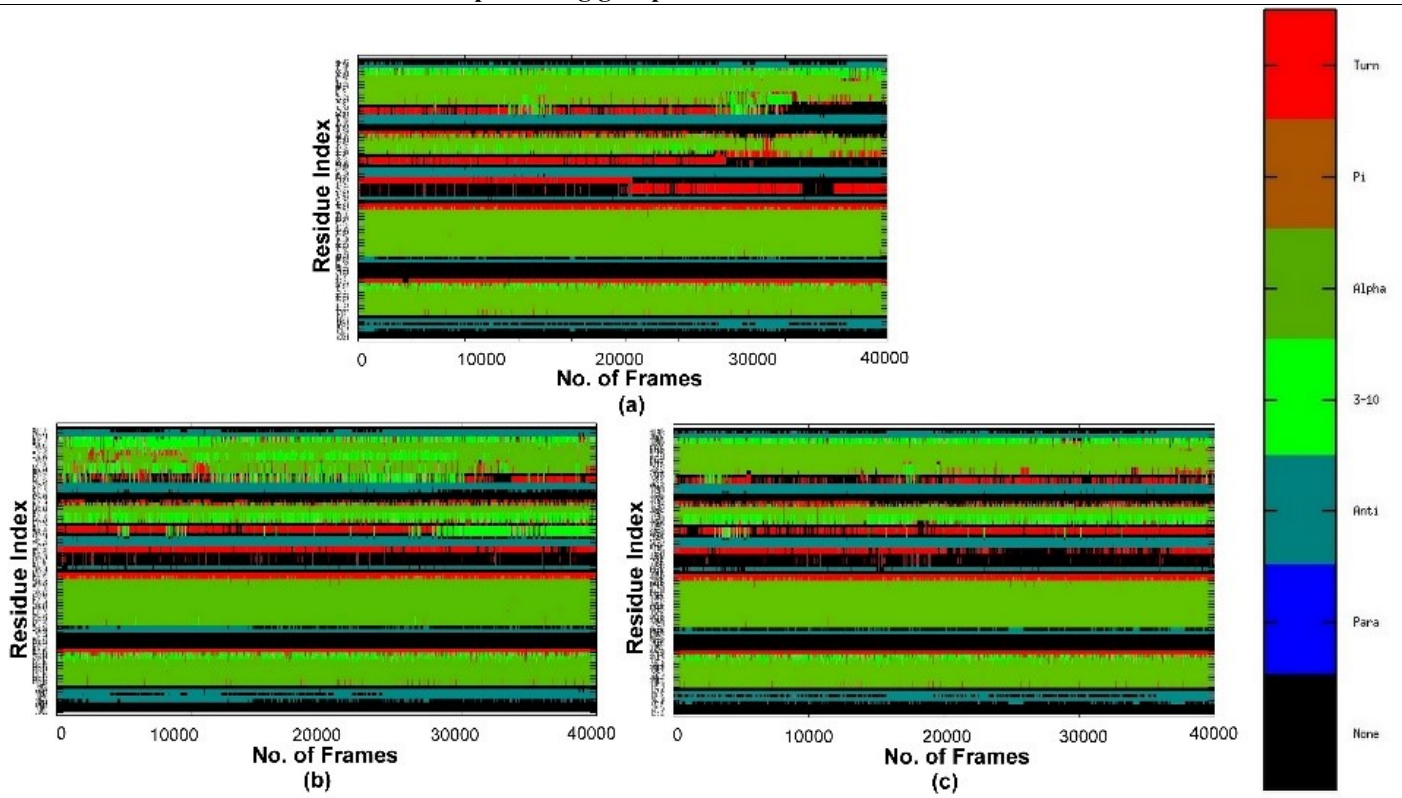

Figure 8. The evolution of secondary structure evaluated using DSSP is shown for MDM2 molecule in (a) Apo, (b) complex with idasanutlin, and (c) complex with PPG-idasanutlin. Y-axis depicts MDM2 residues and X-axis depicts time frames during the course of MD simulation. The secondary structure components of p53 are color-coded as shown in the panel.

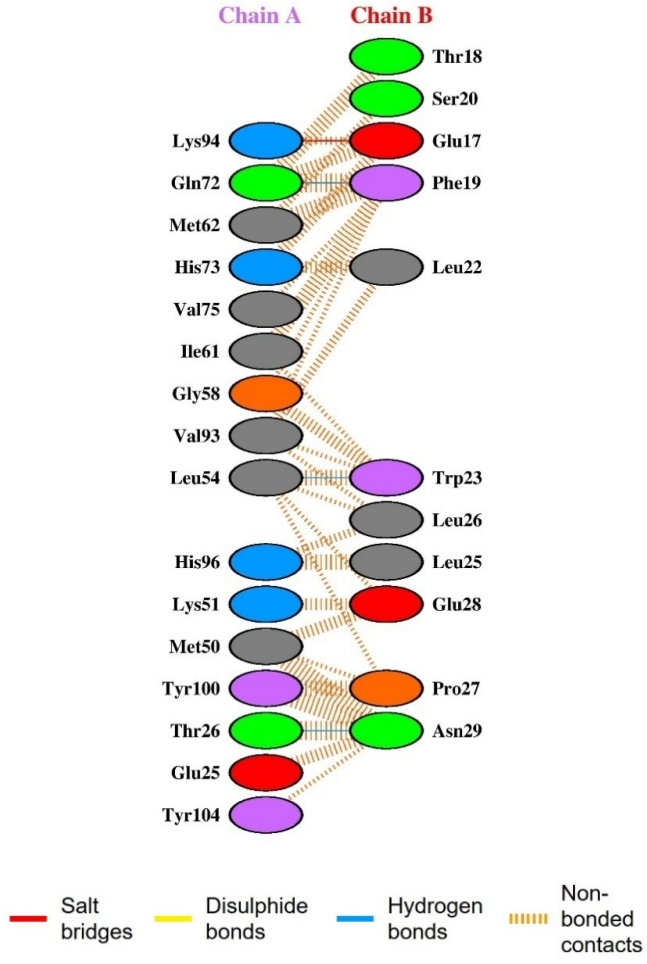

Figure 9. MDM2 (Chain A)-p53 (Chain B) residues interaction profile.

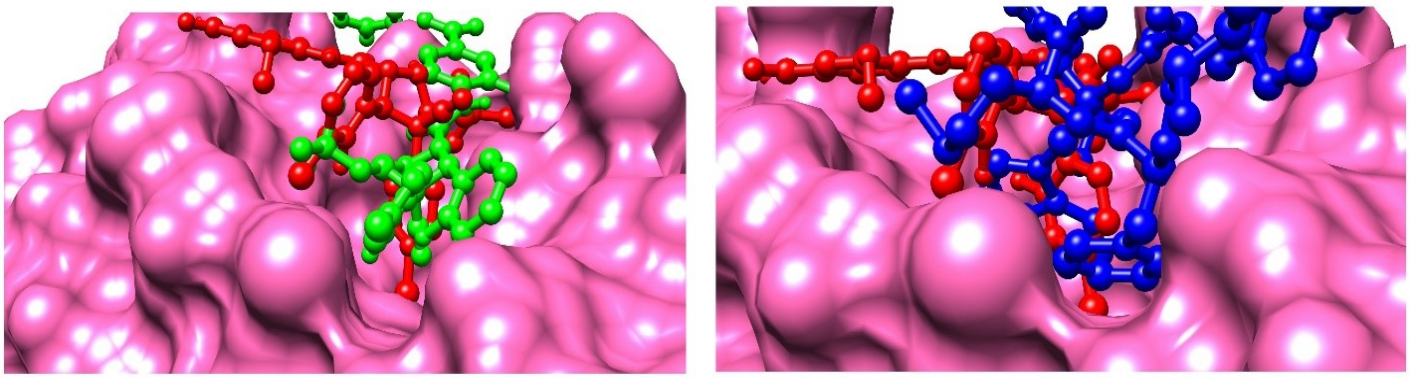

Figure 10. Binding of (a) idasanutlin (red) and PPG-idasanutlin (green); and (b) idasanutlin (red) and p53 (blue) in the binding cavity of MDM2.

Table 1. Average properties of MDM2 (Apo), MDM2-idasanutlin, and MDM2-PPG-idasanutlin throughout the MD simulation.

Average Properties	During Production		
	MDM2 (Apo)	MDM2-idasanutlin	MDM2-PPG-idasanutlin
RMSD	1.44 ± 0.25	1.41 ± 0.15	1.35 ± 0.19
RMSF	0.89 ± 0.42	0.83 ± 0.32	0.79 ± 0.31
Rg	13.04 ± 0.10	13.06 ± 0.07	12.95 ± 0.08
SASA	5777.98 ± 2000.05	5808.40 ± 183.78	5894.16 ± 183.20

Table 2. Residues of MDM2 interacting with p53, idasanutlin, and PPG-idasanutlin.

System	MDM2 interacting residue numbers and residue names
p53 with MDM2 (PDB ID: 1YCR)	25 (GLU), 26 (THR), 50 (MET), 51 (LYS), 54 (LEU), 58 (GLY), 61 (ILE), 62 (MET), 72 (GLN), 73 (HIS), 75 (VAL), 93 (VAL), 94 (LYS), 96 (HIS), 100 (TYR), 104 (TYR)
Idasanutlin with MDM2	54 (LEU), 58 (GLY), 61 (ILE), 62 (MET), 67 (TYR), 72 (GLN), 73 (HIS), 75 (VAL), 93 (VAL), 94 (LYS)
PPG-idasanutlin with MDM2	54 (LEU), 55 (PHE), 57 (LEU), 58 (GLY), 59 (GLN), 61 (ILE), 62 (MET), 63 (THR), 93 (VAL), 96 (HIS), 99 (ILE)
Common MDM2 interacting residues between p53 and Idasanutlin	54 (LEU), 58 (GLY), 61 (ILE), 62 (MET), 72 (GLN), 73 (HIS), 75 (VAL), 93 (VAL), 94 (LYS)
Common MDM2 interacting residues between p53 and PPG-idasanutlin	54 (LEU), 58 (GLY), 61 (ILE), 62 (MET), 93 (VAL), 96 (HIS)

4. CONCLUSIONS

Here in this study, we have demonstrated the molecular interactions between MDM2 and its photactivatable inhibitor. The active inhibitor, idasanutlin when it is free from PPG, fits properly into the binding cavity of MDM2. α-helices, which aid in the stability of a protein, are much abundant in the MDM2-idasanutlin complex than in the MDM2-PPG-idasanutlin complex. Also from the interaction profiles of MDM2-p53, MDM2-idasanutlin and MDM2-PPG-idasanutlin complexes, we noticed p53 and the active inhibitor, idasanutlin free from PPG, to interact with nearly the same residues in MDM2. Our findings in this study can be useful in designing more potent photoactivatable MDM2 inhibitors improving the efficiency of cancer chemotherapy.

5. REFERENCES

1. Bild, A.H.; Yao, G.; Chang, J.T.; Wang, Q.; Potti, A.; Chasse, D.; Joshi, M.B.; Harpole, D.; Lancaster, J.M.; Berchuck, A.; Olson Jr, J.A. Oncogenic pathway signatures in human cancers as a guide to targeted therapies. *Nature* **2006**, *439*, 353, https://doi.org/10.1038/nature04296.
2. Moslehi, J.J. Cardiovascular toxic effects of targeted cancer therapies. *N. Engl. J. Med.* **2016**, *375*, 1457-1467, https://doi.org/10.1056/nejmra1100265.
3. Van't Veer, L.J.; Bernards, R. Enabling personalized cancer medicine through analysis of gene-expression patterns. *Nature* **2008**, *452*, 564, https://doi.org/10.1038/nature06915.
4. Kastenhuber, E.R.; Lowe, S.W. Putting p53 in context. *Cell* **2017**, *170*, 1062-1078, https://doi.org/10.1016/j.cell.2017.08.028.
5. Vogelstein, B.; Kinzler, K.W. p53 function and dysfunction. *Cell* **1992**, *70*, 523-526, https://doi.org/10.1016/0092-8674(92)90421-8.
6. Brown, C.J.; Lain, S.; Verma, C.S.; Fersht, A.R.; Lane, D.P. Awakening guardian angels: drugging the p53 pathway. *Nat. Rev. Cancer* **2009**, *9*, 862, https://doi.org/10.1038/nrc2763.
7. Burgess, A.; Chia, K.M.; Haupt, S.; Thomas, D.; Haupt, Y.; Lim, E. Clinical overview of MDM2/X-targeted therapies. *Frontiers in oncology* **2016**, *6*, 7, https://doi.org/10.3389/fonc.2016.00007.
8. Krenning, L.; Feringa, F.M.; Shaltiel, I.A.; van den Berg, J.; Medema, R.H. Transient activation of p53 in G2 phase is sufficient to induce senescence. *Mol. Cell* **2014**, *55*, 59-72, https://doi.org/10.1016/j.molcel.2014.05.007.

9. Lakoma, A.; Barbieri, E.; Agarwal, S.; Jackson, J.; Chen, Z.; Kim, Y.; McVay, M.; Shohet, J.M.; Kim, E.S. The MDM2 small-molecule inhibitor RG7388 leads to potent tumor inhibition in p53 wild-type neuroblastoma. *Cell death discovery* **2015**, *1*, 15026, https://doi.org/10.1038/cddiscovery.2015.26.
10. Haupt, Y.; Maya, R.; Kazaz, A.; Oren, M. Mdm2 promotes the rapid degradation of p53. *Nature* **1997**, *387*, 296, https://doi.org/10.1038/387296a0.
11. Honda, R.; Tanaka, H.; Yasuda, H. Oncoprotein MDM2 is a ubiquitin ligase E3 for tumor suppressor p53. *FEBS Lett.* **1997**, *420*, 25-27, https://doi.org/10.1016/s0014-5793(97)01480-4.
12. Kubbutat, M.H.; Jones, S.N.; Vousden, K.H. Regulation of p53 stability by Mdm2. *Nature* **1997**, *387*, 299, https://doi.org/10.1038/387299a0.
13. Ye, Q.; Jiang, M.; Huang, W.T.; Ling, Y.; Olson, S.H.; Sun, D.; Xu, G.; Yan, X.; Wong, B.K.; Jin, L. Pharmacokinetics and metabolism of AMG 232, a novel orally bioavailable inhibitor of the MDM2–p53 interaction, in rats, dogs and monkeys: in vitro–in vivo correlation. *Xenobiotica* **2015**, *45*, 681-692, https://doi.org/10.3109/00498254.2015.1010632
14. Neochoritis, C.; Estrada-Ortiz, N.; Khoury, K.; Dömling, A. p53–MDM2 and MDMX Antagonists. In *Annu. Rep. Med. Chem.* **2014**, *49*, 167-187, https://doi.org/10.1016/b978-0-12-800167-7.00012-2.
15. Huang, W.; Cai, L.; Chen, C.; Xie, X.; Zhao, Q.; Zhao, X.; Zhou, H.Y.; Han, B.; Peng, C. Computational analysis of spiro-oxindole inhibitors of the MDM2-p53 interaction: insights and selection of novel inhibitors. *J. Biomol. Struct. Dyn.* **2016**, *34*, 341-351, https://doi.org/10.1080/07391102.2015.1031178.
16. Harris, S.L.; Levine, A.J. The p53 pathway: positive and negative feedback loops. *Oncogene* **2005**, *24*, 2899, https://doi.org/10.1038/sj.onc.1208615.
17. Ray-Coquard, I.; Blay, J.Y.; Italiano, A.; Le Cesne, A.; Penel, N.; Zhi, J.; Heil, F.; Rueger, R.; Graves, B.; Ding, M.; Geho, D. Effect of the MDM2 antagonist RG7112 on the P53 pathway in patients with MDM2-amplified, well-differentiated or dedifferentiated liposarcoma: an exploratory proof-of-mechanism study. *The lancet oncology* **2012**, *13*, 1133-1140, https://doi.org/10.1016/s1470-2045(12)70474-6.
18. Vassilev, L.T.; Vu, B.T.; Graves, B.; Carvajal, D.; Podlaski, F.; Filipovic, Z.; Kong, N.; Kammlott, U.; Lukacs, C.; Klein, C.; Fotouhi, N. In vivo activation of the p53 pathway by small-molecule antagonists of MDM2. *Science* **2004**, *303*, 844-848, https://doi.org/10.1126/science.1092472.
19. Broichhagen, J.; Frank, J.A.; Trauner, D. A roadmap to success in photopharmacology. *Acc. Chem. Res.* **2015**, *48*, 1947-1960, https://doi.org/10.1021/acs.accounts.5b00129.
20. Lerch, M.M.; Hansen, M.J.; van Dam, G.M.; Szymanski, W.; Feringa, B.L. Emerging targets in photopharmacology. *Angewandte Chemie International Edition* **2016**, *55*, 10978-10999, https://doi.org/10.1002/anie.201601931.
21. Gandioso, A.; Cano, M.; Massaguer, A.; Marchán, V. A green light-triggerable RGD peptide for photocontrolled targeted drug delivery: synthesis and photolysis studies. *The Journal of organic chemistry* **2016**, *81*, 11556-11564, https://doi.org/10.1021/acs.joc.6b02415.
22. Stanton-Humphreys, M.N.; Taylor, R.D.; McDougall, C.; Hart, M.L.; Brown, C.T.A.; Emptage, N.J.; Conway, S.J. Wavelength-orthogonal photolysis of neurotransmitters in vitro. *Chemical Communications* **2012**, *48*, 657-659, https://doi.org/10.1039/c1cc15135e.
23. Velema, W.A.; van der Berg, J.P.; Szymanski, W.; Driessen, A.J.; Feringa, B.L. Orthogonal control of antibacterial activity with light. *ACS Chem. Biol.* **2014**, *9*, 1969-1974, https://doi.org/10.1021/cb500313f.
24. Hansen, M.J.; Velema, W.A.; Lerch, M.M.; Szymanski, W.; Feringa, B.L. Wavelength-selective cleavage of photoprotecting groups: strategies and applications in dynamic systems. *Chem. Soc. Rev.* **2015**, *44*, 3358-3377, https://doi.org/10.1039/c5cs00118h.
25. Klán, P.; Solomek, T.; Bochet, C.G.; Blanc, A.; Givens, R.; Rubina, M.; Popik, V.; Kostikov, A.; Wirz, J. Photoremovable protecting groups in chemistry and biology: reaction mechanisms and efficacy. *Chemical reviews* **2012**, *113*, 119-191.
26. Hansen, M.J.; Feringa, F.M.; Kobauri, P.; Szymanski, W.; Medema, R.H.; Feringa, B.L. Photoactivation of MDM2 Inhibitors: Controlling Protein–Protein Interaction with Light. *J. Am. Chem. Soc.* **2018**, *140*, 13136-13141, https://doi.org/10.1021/jacs.8b04870.
27. Berman, H.M.; Westbrook, J.; Feng, Z.; Gilliland, G.; Bhat, T.N.; Weissig, H.; Shindyalov, I.N.; Bourne, P.E. The protein data bank. *Nucleic Acids Res.* **2000**, *28*, 235-242, https://doi.org/10.1093/nar/28.1.235.
28. Pettersen, E.F.; Goddard, T.D.; Huang, C.C.; Couch, G.S.; Greenblatt, D.M.; Meng, E.C.; Ferrin, T.E. UCSF Chimera—a visualization system for exploratory research and analysis. *J. Comput. Chem.* **2004**, *25*, 1605-1612, https://doi.org/10.1002/jcc.20084.
29. Bolton, E.E.; Wang, Y.; Thiessen, P.A.; Bryant, S.H. PubChem: integrated platform of small molecules and biological activities. In *Annu. Rep. Comput. Chem.* **2008**, *4*, 217-241, https://doi.org/10.1016/s1574-1400(08)00012-1.
30. O'Boyle, N. M.; Banck, M.; James, C. A.; Morley, C.; Vandermeersch, T.; Hutchison, G.R. Open Babel: An open chemical toolbox. *J. Cheminf.* **2011**, *3*, 33, https://doi.org/10.1186/1758-2946-3-33.
31. Smith, T.J. MolView: a program for analyzing and displaying atomic structures on the Macintosh personal computer. *J. Mol. Graphics* **1995**, *13*, 122-125, https://doi.org/10.1016/0263-7855(94)00019-o.
32. Thompson, M.A. ArgusLab 4.0. 1. *Planaria Software LLC, Seattle, WA* 2004.
33. Schneidman-Duhovny, D.; Inbar, Y.; Nussinov, R.; Wolfson, H.J. PatchDock and SymmDock: servers for rigid and symmetric docking. *Nucleic Acids Res.* **2005**, *33*(suppl_2), W363-W367, https://doi.org/10.1093/nar/gki481.
34. Maiorov, V.N.; Crippen, G.M. Significance of root-mean-square deviation in comparing three-dimensional structures of globular proteins. *J. Mol. Biol.* **1994**, *235*, 625-634. https://doi.org/10.1006/jmbi.1994.1017
35. Case, D. A.; Babin, V.; Berryman, J. T.; Betz, R. M.; Cai, Q.; Cerutti, D. S.; Cheatham, T. E.; Darden, T. A.; Duke, R. E.; Gohlke, H.; Goetz, A. W.; Gusarov, S.; Homeyer, N.; Janowski, P.; Kaus, J.; Kolossváry, I.; Kovalenko, A.; Lee, T. S.; LeGrand, S.; Luchko, T.; Luo, R.; Madej, B.; Merz, K. M.; Paesani, F.; Roe, D. R.; Roitberg, A.; Sagui, C.; Salomon-Ferrer, R.; Seabra, G.; Simmerling, C. L.; Smith, W.; Swails, J.; Walker, R. C.; Wang, J.; Wolf, R. M.; Wu, X.; Kollman, P. A. AMBER 14. *University of California: San Francisco* 2014.
36. Hornak, V.; Abel, R.; Okur, A.; Strockbine, B.; Roitberg, A.; Simmerling, C. Comparison of multiple Amber force fields and development of improved protein backbone parameters. *Proteins: Struct., Funct., Bioinf.* **2006**, *65*, 712-725, https://doi.org/10.1002/prot.21123.
37. Wang, J.; Wolf, R.M.; Caldwell, J.W.; Kollman, P.A.; Case, D.A. Development and testing of a general amber force field. *J. Comput. Chem.* **2004**, *25*, 1157-1174, https://doi.org/10.1002/jcc.20035.
38. Wang, J.; Wang, W.; Kollman, P.A.; Case, D.A. Antechamber: an accessory software package for molecular

mechanical calculations. *J. Am. Chem. Soc* **2001**, *222*, U403, https://doi.org/10.1021/ja003164o.
39. Darden, T.; York, D.; Pedersen, L. Particle mesh Ewald: An N· log (N) method for Ewald sums in large systems. *J. Chem. Phys.* **1993**, *98*, 10089-10092, https://doi.org/10.1063/1.464397.
40. Salomon-Ferrer, R.; Götz, A.W.; Poole, D.; Le Grand, S.; Walker, R.C. Routine microsecond molecular dynamics simulations with AMBER on GPUs. 2. Explicit solvent particle mesh Ewald. *J. Chem. Theory Comput.* **2013**, *9*, 3878-3888, https://doi.org/10.1021/ct400314y.
41. Lemak, A.S.; Balabaev, N.K. On the Berendsen thermostat. *Mol. Simul.* **1994**, *13*, 177-187, https://doi.org/10.1080/08927029408021981.
42. Ryckaert, J.P.; Ciccotti, G.; Berendsen, H.J. Numerical integration of the cartesian equations of motion of a system with constraints: molecular dynamics of n-alkanes. *J. Comput. Phys.* **1977**,*23*, 327-341, https://doi.org/10.1016/0021-9991(77)90098-5.
43. Roe, D.R.; Cheatham III, T.E. PTRAJ and CPPTRAJ: software for processing and analysis of molecular dynamics trajectory data. *J. Chem. Theory Comput.* **2013**, *9*, 3084-3095, https://doi.org/10.1021/ct400341p.
44. Humphrey, W.; Dalke, A.; Schulten, K. VMD: visual molecular dynamics. *J. Mol. Graphics* **1996**, *14*, 33-38, https://doi.org/10.1016/0263-7855(96)00018-5.
45. De Beer, T.A.; Berka, K.; Thornton, J.M.; Laskowski, R.A. PDBsum additions. *Nucleic Acids Res.* **2013**, *42*(D1), D292-D296, https://doi.org/10.1093/nar/gkt940.
46. Laskowski, R.A. PDBsum: summaries and analyses of PDB structures. *Nucleic Acids Res.* **2001**, *29*, 221-222, https://doi.org/10.1093/nar/29.1.221.
47. Laskowski, R.A.; Hutchinson, E.G.; Michie, A.D.; Wallace, A.C.; Jones, M.L.; Thornton, J.M. PDBsum: a Web-based database of summaries and analyses of all PDB structures. *Trends Biochem. Sci.* **1997**, *22*, 488-490, https://doi.org/10.1016/s0968-0004(97)01140-7.
48. Baker, E.N.; Hubbard, R.E. Hydrogen bonding in globular proteins. *Prog. Biophys. Mol. Biol.* **1984**, *44*, 97-179, https://doi.org/10.1016/0079-6107(84)90007-5.
49. Kabsch, W.; Sander, C. Dictionary of protein secondary structure: pattern recognition of hydrogen-bonded and geometrical features. *Biopolymers* **1983**, *22*, 2577-2637, https://doi.org/10.1002/bip.360221211.
50. Meng, E.C.; Pettersen, E.F.; Couch, G.S.; Huang, C.C.; Ferrin, T.E. Tools for integrated sequence-structure analysis with UCSF Chimera. *BMC bioinformatics* **2006**, *7*, 339, https://doi.org/10.1186/1471-2105-7-339.

6. ACKNOWLEDGEMENTS

The authors extend their deepest gratitude to Tezpur University and University Grants Commission, India, for the start-up grant. They also thank Ms. Priyanka Borah and Ms. Navamallika Dutta for doing the necessary English corrections.

Supplementary Figures

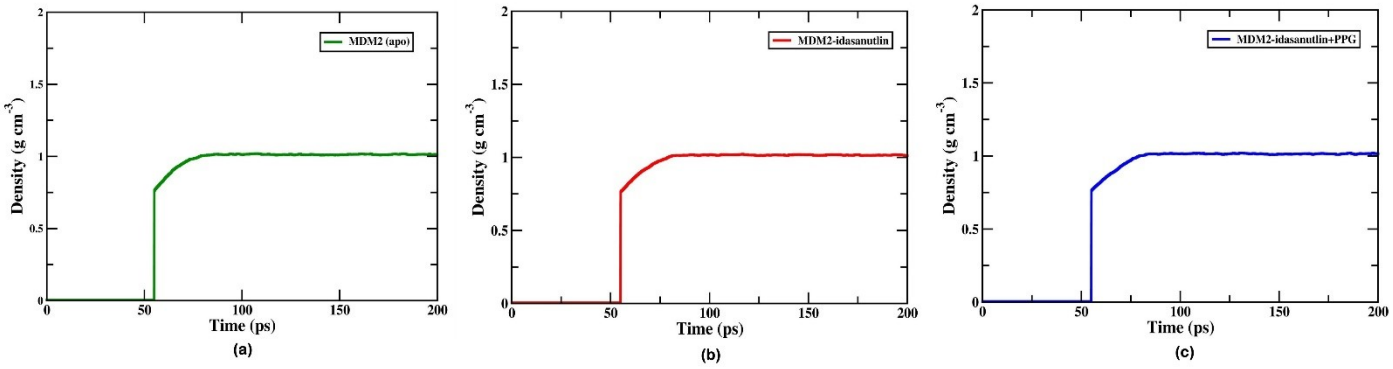

Figure S1. Assessment of stability of MD parameters: Density during the equilibration phases of MD simulation for (i) MDM2 (Apo), (ii) MDM2-idasanutlin, and (iii) MDM2-PPG-idasanutlin systems.

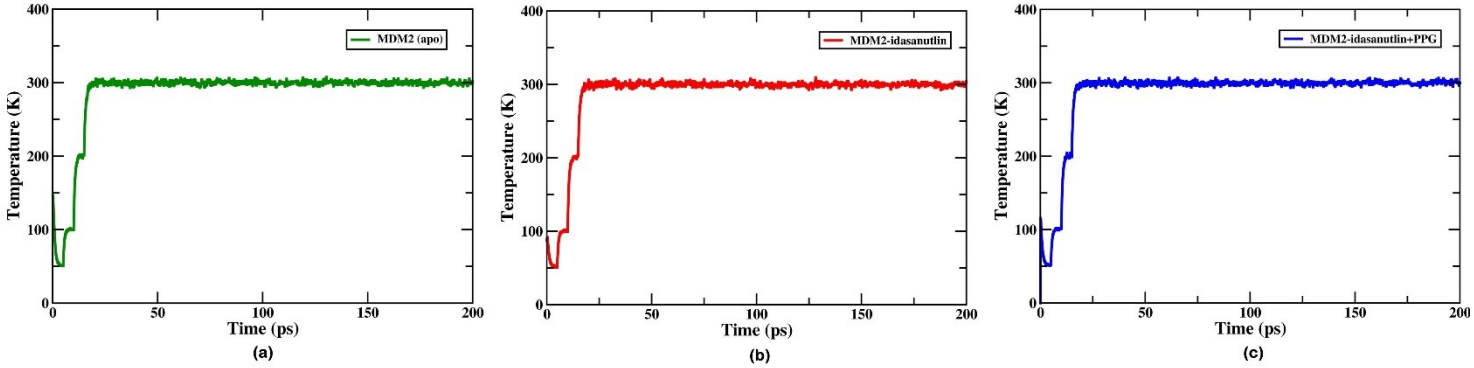

Figure S2. Assessment of stability of MD parameters: Temperature during the equilibration phases of MD simulation for (i) MDM2 (Apo), (ii) MDM2-idasanutlin, and (iii) MDM2-PPG-idasanutlin systems.

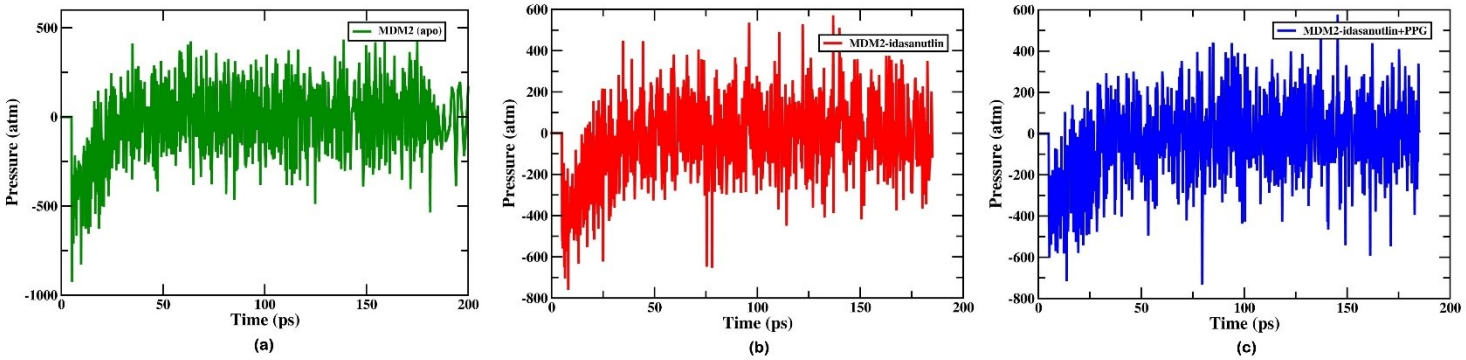

Figure S3. Assessment of stability of MD parameters: Pressure during the equilibration phases of MD simulation for (i) MDM2 (Apo), (ii) MDM2-idasanutlin, and (iii) MDM2-PPG-idasanutlin systems.

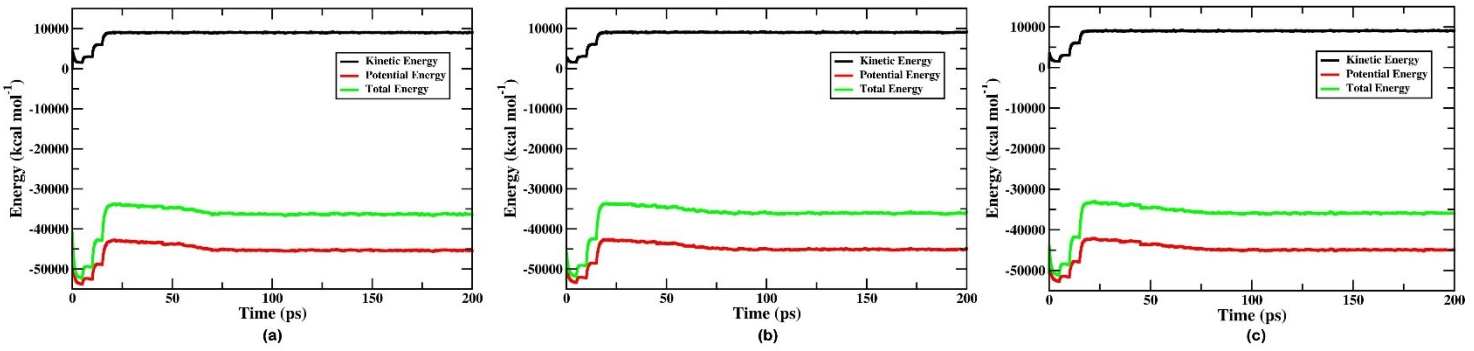

Figure S4. Assessment of stability of MD parameters: Energy during the equilibration phases of MD simulation for (i) MDM2 (Apo), (ii) MDM2-idasanutlin, and (iii) MDM2-PPG-idasanutlin systems.

Supplementary Tables

Table S1. List of atom-atom interactions across the MDM2-idasanutlin interface.

Non-bonded contacts

	<----- MDM2 ----->						<----- IDASANUTLIN ----->					
	Atom no.	Atom name	Res name	Res no.	Chain		Atom no.	Atom name	Res name	Res no.	Chain	Distance (Å)
1.	233	C	LEU	54	A	---	12	C	LIG	1		3.86
2.	234	O	LEU	54	A	---	5	O	LIG	1		3.72
3.	234	O	LEU	54	A	---	12	C	LIG	1		3.56
4.	234	O	LEU	54	A	---	12	C	LIG	1		3.64
5.	235	CB	LEU	54	A	---	12	C	LIG	1		3.79
6.	271	CA	GLY	58	A	---	9	N	LIG	1		3.59
7.	301	CG2	ILE	61	A	---	9	N	LIG	1		3.79
8.	302	CD1	ILE	61	A	---	12	C	LIG	1		3.62
9.	302	CD1	ILE	61	A	---	12	C	LIG	1		3.07
10.	308	CG	MET	62	A	---	9	N	LIG	1		3.32
11.	308	CG	MET	62	A	---	12	C	LIG	1		3.90
12.	309	SD	MET	62	A	---	5	O	LIG	1		3.89
13.	309	SD	MET	62	A	---	9	N	LIG	1		3.52
14.	309	SD	MET	62	A	---	12	C	LIG	1		3.72
15.	310	CE	MET	62	A	---	5	O	LIG	1		2.39
16.	310	CE	MET	62	A	---	9	N	LIG	1		2.90
17.	310	CE	MET	62	A	---	9	N	LIG	1		3.14
18.	310	CE	MET	62	A	---	12	C	LIG	1		2.89
19.	310	CE	MET	62	A	---	12	C	LIG	1		2.39
20.	350	CB	TYR	67	A	---	9	N	LIG	1		3.74
21.	396	O	GLN	72	A	---	9	N	LIG	1		3.85
22.	396	O	GLN	72	A	---	12	C	LIG	1		3.39
23.	396	O	GLN	72	A	---	12	C	LIG	1		3.77
24.	399	CD	GLN	72	A	---	12	C	LIG	1		3.62
25.	400	OE1	GLN	72	A	---	12	C	LIG	1		3.76
26.	400	OE1	GLN	72	A	---	12	C	LIG	1		2.40
27.	403	CA	HIS	73	A	---	12	C	LIG	1		3.88
28.	403	CA	HIS	73	A	---	12	C	LIG	1		3.34
29.	406	CB	HIS	73	A	---	12	C	LIG	1		3.61
30.	426	CG2	VAL	75	A	---	9	N	LIG	1		3.82
31.	556	CA	VAL	93	A	---	1	CL	LIG	1		3.81
32.	558	O	VAL	93	A	---	1	CL	LIG	1		3.58
33.	559	CB	VAL	93	A	---	1	CL	LIG	1		3.23
34.	559	CB	VAL	93	A	---	3	F	LIG	1		3.70
35.	559	CB	VAL	93	A	---	12	C	LIG	1		3.63
36.	559	CB	VAL	93	A	---	12	C	LIG	1		3.59
37.	559	CB	VAL	93	A	---	12	C	LIG	1		3.57
38.	559	CB	VAL	93	A	---	12	C	LIG	1		3.30
39.	560	CG1	VAL	93	A	---	1	CL	LIG	1		3.83
40.	560	CG1	VAL	93	A	---	12	C	LIG	1		3.89
41.	560	CG1	VAL	93	A	---	12	C	LIG	1		3.49
42.	560	CG1	VAL	93	A	---	12	C	LIG	1		3.49
43.	560	CG1	VAL	93	A	---	12	C	LIG	1		3.23
44.	560	CG1	VAL	93	A	---	12	C	LIG	1		3.80
45.	560	CG1	VAL	93	A	---	12	C	LIG	1		3.41
46.	561	CG2	VAL	93	A	---	1	CL	LIG	1		3.64
47.	561	CG2	VAL	93	A	---	3	F	LIG	1		3.77
48.	561	CG2	VAL	93	A	---	12	C	LIG	1		3.77
49.	561	CG2	VAL	93	A	---	12	C	LIG	1		2.79
50.	561	CG2	VAL	93	A	---	12	C	LIG	1		3.85
51.	561	CG2	VAL	93	A	---	12	C	LIG	1		2.28
52.	561	CG2	VAL	93	A	---	12	C	LIG	1		2.95
53.	567	CG	LYS	94	A	---	1	CL	LIG	1		3.78

Number of non-bonded contacts: 53

Table S2. List of atom-atom interactions across the MDM2-PPG-idasanutlin interface.

Non-bonded contacts											
	<----- MDM2 ----->					<----- PPG-IDASANUTLIN ----->					
	Atom no.	Atom name	Res name	Res no.	Chain		Atom no.	Atom name	Res name	Res no.	Chain	Distance (Å)
1.	232	CA	LEU	54	A	---	8	F	LIG	1		3.68
2.	232	CA	LEU	54	A	---	12	N	LIG	1		3.78
3.	233	C	LEU	54	A	---	19	O	LIG	1		3.23
4.	234	O	LEU	54	A	---	2	C	LIG	1		3.90
5.	234	O	LEU	54	A	---	2	C	LIG	1		3.56
6.	234	O	LEU	54	A	---	19	O	LIG	1		3.18
7.	234	O	LEU	54	A	---	2	C	LIG	1		3.43
8.	234	O	LEU	54	A	---	12	N	LIG	1		3.21
9.	235	CB	LEU	54	A	---	2	C	LIG	1		3.83
10.	235	CB	LEU	54	A	---	8	F	LIG	1		2.79
11.	235	CB	LEU	54	A	---	2	C	LIG	1		3.73
12.	235	CB	LEU	54	A	---	19	O	LIG	1		3.47
13.	236	CG	LEU	54	A	---	2	C	LIG	1		3.72
14.	236	CG	LEU	54	A	---	2	C	LIG	1		3.47
15.	236	CG	LEU	54	A	---	8	F	LIG	1		2.36
16.	237	CD1	LEU	54	A	---	2	C	LIG	1		3.09
17.	237	CD1	LEU	54	A	---	2	C	LIG	1		2.88
18.	237	CD1	LEU	54	A	---	2	C	LIG	1		3.01
19.	237	CD1	LEU	54	A	---	2	C	LIG	1		3.43
20.	237	CD1	LEU	54	A	---	2	C	LIG	1		3.76
21.	237	CD1	LEU	54	A	---	2	C	LIG	1		3.34
22.	237	CD1	LEU	54	A	---	8	F	LIG	1		2.76
23.	238	CD2	LEU	54	A	---	1	CL	LIG	1		3.57
24.	238	CD2	LEU	54	A	---	2	C	LIG	1		3.21
25.	238	CD2	LEU	54	A	---	2	C	LIG	1		3.87
26.	238	CD2	LEU	54	A	---	2	C	LIG	1		2.80
27.	238	CD2	LEU	54	A	---	8	F	LIG	1		1.53
28.	238	CD2	LEU	54	A	---	2	C	LIG	1		3.64
29.	238	CD2	LEU	54	A	---	12	N	LIG	1		3.75
30.	238	CD2	LEU	54	A	---	2	C	LIG	1		3.87
31.	239	N	PHE	55	A	---	19	O	LIG	1		3.36
32.	240	CA	PHE	55	A	---	19	O	LIG	1		3.50
33.	242	O	PHE	55	A	---	2	C	LIG	1		3.64
34.	242	O	PHE	55	A	---	2	C	LIG	1		3.79
35.	244	CG	PHE	55	A	---	2	C	LIG	1		3.78
36.	245	CD1	PHE	55	A	---	2	C	LIG	1		3.89
37.	245	CD1	PHE	55	A	---	2	C	LIG	1		3.13
38.	245	CD1	PHE	55	A	---	2	C	LIG	1		2.48
39.	245	CD1	PHE	55	A	---	2	C	LIG	1		2.62
40.	245	CD1	PHE	55	A	---	19	O	LIG	1		2.93
41.	245	CD1	PHE	55	A	---	19	O	LIG	1		3.34
42.	245	CD1	PHE	55	A	---	2	C	LIG	1		2.82
43.	245	CD1	PHE	55	A	---	2	C	LIG	1		3.67
44.	247	CE1	PHE	55	A	---	2	C	LIG	1		3.29
45.	247	CE1	PHE	55	A	---	2	C	LIG	1		2.60
46.	247	CE1	PHE	55	A	---	2	C	LIG	1		1.96
47.	247	CE1	PHE	55	A	---	19	O	LIG	1		2.26
48.	247	CE1	PHE	55	A	---	19	O	LIG	1		2.33
49.	247	CE1	PHE	55	A	---	2	C	LIG	1		3.04
50.	247	CE1	PHE	55	A	---	2	C	LIG	1		3.39
51.	249	CZ	PHE	55	A	---	2	C	LIG	1		3.14
52.	249	CZ	PHE	55	A	---	19	O	LIG	1		3.28
53.	249	CZ	PHE	55	A	---	19	O	LIG	1		3.07
54.	249	CZ	PHE	55	A	---	2	C	LIG	1		3.24
55.	249	CZ	PHE	55	A	---	2	C	LIG	1		3.84
56.	249	CZ	PHE	55	A	---	2	C	LIG	1		3.88
57.	266	CB	LEU	57	A	---	12	N	LIG	1		3.55
58.	267	CG	LEU	57	A	---	12	N	LIG	1		3.62
59.	269	CD2	LEU	57	A	---	12	N	LIG	1		3.82
60.	270	N	GLY	58	A	---	12	N	LIG	1		3.70
61.	271	CA	GLY	58	A	---	2	C	LIG	1		3.78
62.	280	CD	GLN	59	A	---	2	C	LIG	1		3.71
63.	280	CD	GLN	59	A	---	19	O	LIG	1		3.52
64.	280	CD	GLN	59	A	---	2	C	LIG	1		3.38

65.	280	CD	GLN	59	A	---	2	C	LIG	1	3.30
66.	280	CD	GLN	59	A	---	2	C	LIG	1	3.05
67.	280	CD	GLN	59	A	---	2	C	LIG	1	3.39
68.	280	CD	GLN	59	A	---	2	C	LIG	1	3.88
69.	281	OE1	GLN	59	A	---	19	O	LIG	1	3.81
70.	281	OE1	GLN	59	A	---	2	C	LIG	1	2.83
71.	281	OE1	GLN	59	A	---	2	C	LIG	1	3.16
72.	281	OE1	GLN	59	A	---	2	C	LIG	1	3.21
73.	281	OE1	GLN	59	A	---	19	O	LIG	1	2.78
74.	281	OE1	GLN	59	A	---	2	C	LIG	1	2.22
75.	281	OE1	GLN	59	A	---	2	C	LIG	1	2.36
76.	281	OE1	GLN	59	A	---	2	C	LIG	1	3.08
77.	281	OE1	GLN	59	A	---	2	C	LIG	1	3.59
78.	281	OE1	GLN	59	A	---	2	C	LIG	1	3.57
79.	281	OE1	GLN	59	A	---	2	C	LIG	1	2.94
80.	282	NE2	GLN	59	A	---	2	C	LIG	1	3.43
81.	282	NE2	GLN	59	A	---	2	C	LIG	1	2.72
82.	282	NE2	GLN	59	A	---	2	C	LIG	1	3.77
83.	282	NE2	GLN	59	A	---	19	O	LIG	1	3.19
84.	282	NE2	GLN	59	A	---	2	C	LIG	1	3.69
85.	282	NE2	GLN	59	A	---	2	C	LIG	1	3.77
86.	282	NE2	GLN	59	A	---	2	C	LIG	1	3.19
87.	282	NE2	GLN	59	A	---	2	C	LIG	1	2.96
88.	282	NE2	GLN	59	A	---	2	C	LIG	1	3.39
89.	302	CD1	ILE	61	A	---	2	C	LIG	1	3.40
90.	305	C	MET	62	A	---	2	C	LIG	1	3.80
91.	307	CB	MET	62	A	---	2	C	LIG	1	3.76
92.	308	CG	MET	62	A	---	2	C	LIG	1	3.85
93.	309	SD	MET	62	A	---	2	C	LIG	1	3.25
94.	310	CE	MET	62	A	---	2	C	LIG	1	3.58
95.	310	CE	MET	62	A	---	2	C	LIG	1	3.79
96.	311	N	THR	63	A	---	2	C	LIG	1	3.51
97.	312	CA	THR	63	A	---	2	C	LIG	1	3.49
98.	316	OG1	THR	63	A	---	2	C	LIG	1	3.16
99.	558	O	VAL	93	A	---	2	C	LIG	1	3.80
100.	558	O	VAL	93	A	---	1	CL	LIG	1	3.58
101.	559	CB	VAL	93	A	---	2	C	LIG	1	3.69
102.	560	CG1	VAL	93	A	---	2	C	LIG	1	2.94
103.	585	CG	HIS	96	A	---	1	CL	LIG	1	3.09
104.	586	ND1	HIS	96	A	---	2	C	LIG	1	3.61
105.	586	ND1	HIS	96	A	---	1	CL	LIG	1	1.99
106.	587	CD2	HIS	96	A	---	1	CL	LIG	1	3.70
107.	588	CE1	HIS	96	A	---	2	C	LIG	1	3.84
108.	588	CE1	HIS	96	A	---	1	CL	LIG	1	2.20
109.	589	NE2	HIS	96	A	---	1	CL	LIG	1	3.26
110.	616	CG2	ILE	99	A	---	2	C	LIG	1	3.79
111.	616	CG2	ILE	99	A	---	2	C	LIG	1	3.68
112.	616	CG2	ILE	99	A	---	8	F	LIG	1	2.89
Number of non-bonded contacts: 112											